From Electrode Materials to Dynamic Models of Li-ion Cells

An Undergraduate Honors Thesis

Submitted to the Department of Mechanical Engineering

The Ohio State University

In Partial Fulfillment of the Requirements

for Graduation with Distinction in Mechanical Engineering

Bo Jiang

Spring, 2013

Dr. G Rizzoni, Advisor

Abstract

Batteries play a fundamental role in electric vehicles, and help to reduce the environmental impact associated with fossil fuels. Li-ion battery is a promising candidate for vehicles due to its specific energy. This project is focused on experimental characterization and modeling of Li-ion batteries, and the objectives are to analyze battery aging at an electrode level and to better predict battery performance.

The project consists of fabricating half cells of Lithium Iron Phosphate coin cells from unaged and batteries aged under different conditions, and measuring relevant parameters including capacity, state of charge, impedance, and open-circuit voltage.

An equivalent circuit was developed from charging and discharging profile and impedance measurements with parameters calibrated to model the cell behavior. The governing equation of the non-linear system can be approximated by a Pade function with second-order numerator and denominator. The disadvantage of Pade function is that coefficients in the function do not have a physical meaning. The simple equivalent circuit and the linear Pade function will allow fast calculations during design and prediction, and improve the efficiency of predictive maintenance.

ACKNOWLEDGEMENTS

I would first and foremost like to thank Dr. Giorgio Rizzoni. He gave me a last minute chance for undergraduate honors research and introduced me to this project. He was not only a knowledgeable professor, but also a caring and encouraging advisor. Busy as he is, he always takes time to guide me. Outside of this project, he tries to give me the best graduate school research and scholarship opportunities. I always feel lucky to have him as my advisor.

A huge thank you goes to Dr. Shrikant Nagpure. He taught me all the experimental procedures, explained details of the projects, and worked during weekends just to keep my project moving forward.

I greatly appreciate Mr. Alex Bartlett's help. He has being so generous with his time in replying emails and meeting. He passed down his experiences and set up the outstanding example for me to follow.

Table of Contents:

List of Figures

List of Table

Chapter 1: Introduction

1.1 Motivation for Li-ion battery aging research

The issues related to fossil fuels, including the limited amount, fluctuating prices, and associated environmental problems, are driving people's attention to more efficient usage of fossil fuels. The last two decades have witnessed a great advancement in mass production of Hybrid, Plug-in Hybrid, and Electric Vehicles (HEV, PHEV, and EV). Toyota launched their first generation Prius in Japan in 1997 [1]; the Honda CR-Z made its debut in 2008 in Detroit [2]; the Chevy Volt was introduced in 2007 [3]. They adopt an electric propulsion system to achieve a better fuel economy and reduce emissions.

Rechargeable batteries play a fundamental role in HEV, PHEV and EV. In a hybrid electric vehicle, a battery pack is added to provide propulsion along with the internal combustion engine, while in an EV the battery pack provides all the power. Based on the design of the power train control system, the battery pack is charged and discharged with variable current rates during vehicle operation, posing different requirements and challenges to the battery pack. There has been a significant increase in interest in lithium ion batteries for HEVs due to the demand for high specific energy and specific power [4]. Specific energy describes the nominal battery energy per unit mass, and determines the battery weight to achieve a desired electric range. Specific power is the maximum power available per unit mass, and determines battery weight for a given performance target. [5] The high energy and power density of lithium ion batteries allows the development of lighter vehicles for a given

vehicle range and performance. Of the many materials tested as cathode materials, $LiFePO_4$ (LFP) is a promising candidate. LFP is environmental friendly, inexpensive, and abundant, and LFP material features large capacity, good thermal stability, and little hygroscopicity. [4] In this project, LFP is employed as the cathode material.

As a cell is repeatedly charged and discharged throughout their life, the capacity and power capabilities of the cell degrade, a phenomenon known as aging. Specifically the battery capacity drops after a sufficient number of cycles, and the time a fully charged battery can provide electric power is shortened. The battery voltage also drops more quickly as the battery discharges as a consequence of aging, which has a more significant effect for high current applications. Figure 1 shows typical capacity curves of a battery, with voltage on the vertical axis and time on the horizontal axis. From the figure, it is clear that the capacity diminishes and voltage drops faster as the battery ages.

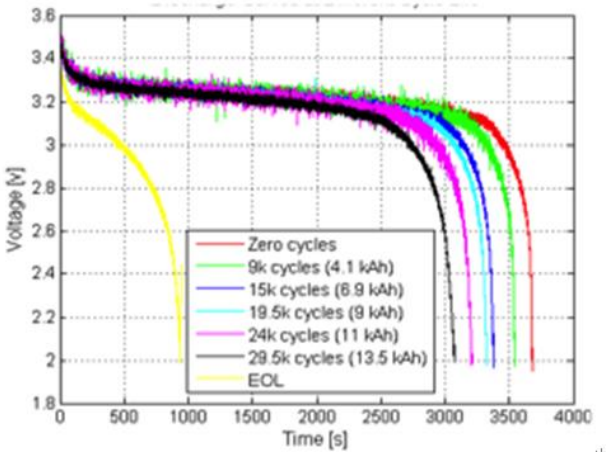

Figure 1: Typical Capacity Curves of a Battery

A battery consists of two electrodes, anode and cathode, separated by an insulating separator and electrolyte. The mechanisms for the aging effect are currently not well

understood; although studies have shown aging is highly dependent on the electrode material, electrolyte, and conditions in which the battery is used [6]. It is generally believed that lithium deposition, electrolyte decomposition, active material dissolution, phase transition inside the insertion electrode materials, and further passive film formation on the electrode and current collectors, all contribute to different degrees of battery aging [7]. Specifically the aging mechanism is different at each electrode. However if only the capacity and power fade of the complete cell are analyzed, the contributions of each electrode cannot be easily discerned from the overall aging. By fabricating coin cells made from each electrode of a deconstructed aged cell, the aging contributions of each electrode can by analyzed separately. With an understanding of the changes experienced by each electrode, may gain insight into the principles behind battery aging, and be able to better predict battery performance. This provides valuable insight in the relationship between the material degradation and system level metrics such as capacity and internal resistance of the cell.

1.2 Objectives

This research project was carried out at the battery aging lab at the Center for Automotive Research. The objectives of the project are listed below.

- To analyze battery aging at an electrode level and to better predict battery performance and improve the efficiency of predictive maintenance;

- To fabricate half cells of Lithium Iron Phosphate coin cells using anode and cathode materials harvested from different locations of new and aged batteries to study the contribution of aging at each electrode to the overall battery aging;
- To cycle coin cells, and to measure relevant parameters including capacity, state of charge, impedance, and open-circuit voltage to understand the changes experienced by parts of each individual electrode during cycling;
- To develop and calibrate separate equivalent circuits for the cathode and anode, with parameters that are functions of temperature, state of charge, location on an electrode, and other aging dependent factors to provide a simple tool for predicting battery performance.

1.3 Overview of thesis

This thesis has 5 chapters. Chapter 2 introduces background. Chapter 3 explains the experimental setup and design. Chapter 4 includes results and discussions. Chapter 5 summarizes the conclusions. Chapter 6 provides recommendation for future work.

Chapter 2: Background

2.1 Circuit models of electrochemical processes

In general a battery does not operate ideally; it involves complicated electrochemical components and processes, and therefore has an internal impedance. There are several physical processes that can cause resistive and energy storage effects in a battery. Most generally, resistive and capacitive behaviors dominate the response of a battery. We first focus on the internal resistance. First of all, electrolyte solution resistance is a significant part of internal impedance of battery. Whenever electrons and charged particles traverse the electrolyte, they face a resistance which depends on the conductivity of the electrolyte and the distance between the electrons. Unfortunately, most cells do not have uniform current distribution through a defined electrolyte area, and determination of the resistance requires specifying the current path and the geometry of electrolyte. Second, as the battery charges and discharges, the potential of the two electrodes may shift, a phenomenon called polarization. Polarization can generate current through an electrochemical reaction at the electrode surface and introduce a polarization resistance. Also there is a resistance associated with charge transfer. Finally, there is an ohmic resistance as the current travels through the electrode matrix and current collector. [8]

A second phenomenon that is necessary to model the behavior of a battery is capacitance. In general, capacitance results from charge separation. Electrochemical reactions occur at surfaces, and the interface between electrode and electrolyte accumulate

opposite charges to form a double layer, which acts like a capacitance.[9] In addition to capacitive effects, one also encounters more complex behavior caused, for example by the phenomenon of diffusion, which cannot be easily explained as a resistive or capacitive behavior. Diffusion can be represented by a so-called Warburg element [10]. Further, the impedance of an electrochemical cell may sometimes appear to follow and inductive behavior, and may require an inductor circuit model to represent its response. [11]

2.2 Advantages of equivalent circuit models

Accounting for the detailed processes of the electrochemical mechanism inside the battery is a lengthy and complicated process, which results in partial differential equations of considerable complexity if modeled from first principles. As an alternative, equivalent circuit modeling is a popular approach to study batteries because it greatly simplifies the modeling process and reduces computational efforts. The approach only requires identifying relatively few parameters and successfully simulates the input-output behavior of a battery. [12]

The equivalent circuit model (ECM) method has been amply described in the literature. Liaw provided some concepts and techniques of ECM. [12] An ECM may have three major components: a static part simulating the thermodynamic properties of electrochemical processes in battery, a dynamic part representing the kinetics of the cell internal impedance, and a source or load for charge and discharge regimes. [12] Such a

circuit is shown in Figure 2. In the circuit, all linear ohmic resistances are combined into R_1, and all faradic, non-linear components are lumped into the CR_2 circuit.

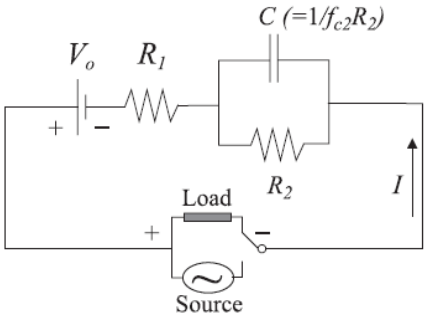

Figure 2: An Equivalent Circuit Model Used to Simulate LiB Performance [12]

Several equivalent circuit models are widely used, including the Rint model, the Thevenin model and the PNGV model, as summarized by H. He. [13] The Rint model implements an ideal voltage source U_{oc} and a resistance R_o, both dependent on SoC, SoH, and temperature. This greatly simplified model only considers the internal resistance of a battery. Figure 3 shows a schematic diagram of the Rint model. The governing equation of the circuit is represented by equation (1).

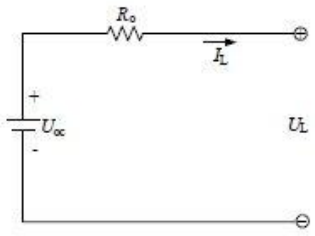

Figure 3: Schematic diagram of the Rint model [13]

$$U_L=U_{OC}-I_LR_o \quad (1)$$

The Thevenin model adds to the Rint model a parallel RC circuit in series with R_o, describing the dynamic characteristics of the battery. Figure 4 shows a schematic diagram of Thevenin model. The system is governed by equations (2) and (3), where U_{OC} stands for open-circuit voltage, R_o and R_{TH} stand for internal resistance and polarization resistance respectively, C_{TH} is the equivalent capacitance, and I_{TH} is the outflow current of C_{TH} [13].

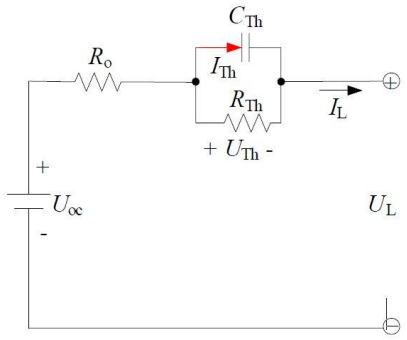

Figure 4: Schematic diagram for the Thevenin model [13]

$$\dot{U}_{TH} = -\frac{U_{TH}}{R_{TH}C_{TH}} + \frac{I_L}{C_{TH}} \tag{2}$$

$$U_L = U_{OC} - U_{TH} - I_L R_o \tag{3}$$

The PNGV model adds a capacitor to the Thevenin model to describe the changing of open circuit voltage generated by the time accumulation of load current, as shown in Figure 5. U_d and U_{PN} are the voltages across capacitors $1/U'_{OC}$ and C_{PN} respectively, and I_{PN} is the outflow current of C_{PN} [13]. The system behavior is described by equation (4) (5) and (6).

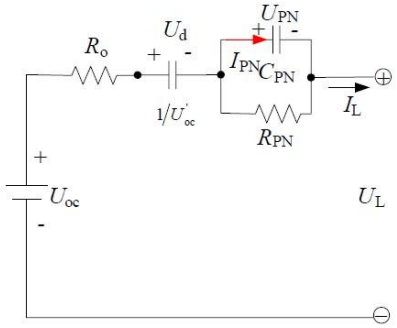

Figure 5: Schematic diagram of the PNGV model [13]

$$\dot{U}_d = U'_{OC} I_L \tag{4}$$

$$\dot{U}_{PN} = -\frac{U_{PN}}{R_{PN} C_{PN}} + \frac{I_L}{C_{PN}} \tag{5}$$

$$U_L = U_{OC} - U_d - U_{PN} - I_L R_o \tag{6}$$

The Thevenin circuit approximately models the polarization of a lithium-ion power battery, but cannot accurately capture the difference between concentration polarization and electrochemical polarization at the end of charge and discharge. To refine the polarization simulation, the Dual Polarization (DP) model adds one more RC circuit to the Thevenin model, as shown in Figure 6 [13]. The equivalent circuit that will be used in this thesis is mainly based on the DP model. The electrical behavior of the DP model can be described by equations (7) (8) and (9). Capacitors C_{pa} and C_{pc} are used to characterize the transient response due to electrochemical and concentration polarization, respectively. U_{pa} and U_{pc} are the voltages across C_{pa} and C_{pc} respectively. I_{pa} and I_{pc} are outflow currents of C_{pa} and C_{pc}, respectively [13].

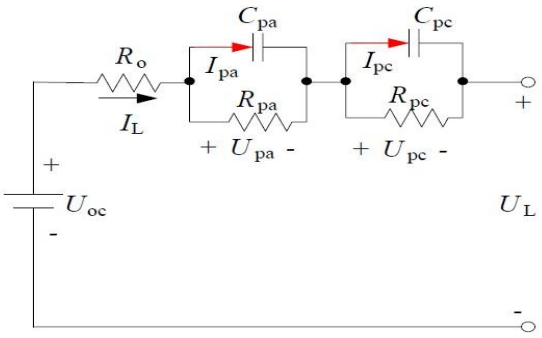

Figure 6: Schematic diagram of the DP model [13]

$$\dot{U}_{pa} = -\frac{U_{PN}}{R_{pa}C_{pa}} + \frac{I_L}{C_{pa}} \tag{7}$$

$$\dot{U}_{pc} = -\frac{U_{pc}}{R_{pc}C_{pc}} + \frac{I_L}{C_{pc}} \tag{8}$$

$$U_L = U_{OC} - U_{pa} - U_{pc} - I_L R_o \tag{9}$$

2.3 Methods of developing equivalent circuit models

Electrochemical Impedance Spectroscopy (EIS) is the main tool used to identify the parameters of an equivalent circuit. EIS is a frequency domain analysis method that generates the Nyquist plot of the cell impedance. EIS is a method based on measuring the sinusoidal frequency response of the cell by imposing a small signal sinusoidal current of variable frequency to the cell, and measuring the resulting voltage response. [10] This analysis is conducted over a broad range of frequencies that can be as low as 0.001 Hz and as high as 100,000 Hz. The results are usually displayed in the form of a Nyquist plot. In a Nyquist plot, the real part of the cell impedance is plotted on the x-axis and the imaginary part on the y-

axis. One drawback of Nyquist plot is that the frequency cannot be seen from the plot. Conventionally EIS has been used to study kinetics in an electrochemical system. Analyses of complex impedance data rely on employing an equivalent circuit to simulate cell performance and behavior, with a series of circuit elements that represent the electrochemical system. [11]

2.4 Related concepts

A few concepts are important in the ECM method. State of charge (SOC) refers to the present available battery capacity as a percentage of maximum capacity. Depth of discharge (DOD) refers to the discharged battery capacity as a percentage of maximum capacity, equals to 1-SOC. There are different concepts related to voltages. Open-circuit voltage is the voltage between battery terminals at equilibrium when no load is applied, and is a function of the state of charge. Terminal voltage is the voltage between battery terminals with load applied, and depends on SOC as well as charge/discharge current. Current rate is a measure of the discharge current relative to its maximum capacity. 1C rate refers to the current at which the battery will fully discharge in one hour. 2C is, therefore, twice the current. [5] Higher discharging current rate appears to accelerate battery aging. According to the study of capacity fade of Sony US 18650 Li-ion batteries cycled using different discharge rates at ambient temperature, the capacity loss after 300 cycles at 2C and 3C discharge rates were estimated to be 13.2% and 16.9% of the initial capacity, while the capacity loss was only 9.5% at 1C [7].

Chapter 3: Experimental Design

3.1 Overview of design

The first stage of this project is fabrication of coin cells using the anode and cathode material harvested from unaged batteries and batteries aged with different current rates. The coin cells are fabricated inside a glove box with a controlled Argon atmosphere. The batteries employ lithium iron phosphate (LFP) as the cathode material and lithium graphite as the anode material. Working electrode designates the electrode being studied, and reference electrode is an experimental reference point for potential measurements. [14] When testing the cathode, the cathode from unaged and aged batteries is used for the working electrode and unaged lithium material is used for reference electrode. When testing the anode, the anode from unaged and aged batteries is used for the working electrode, and unaged lithium material is used for the reference electrode.

Experimental data were collected from the fabricated cell. Each coin cell was subjected to a multi-rate capacity test and electrochemical impedance test (EIS). The data collected with these tests will help in comparing the capacity, impedance, and open circuit voltage of the electrodes harvested from unaged and aged cells. Once enough experimental data is generated, the next step is to develop an equivalent circuit model for the anode and cathode using *Echem Analyst*. *Echem Analyst* is able to calculate unknown parameters to fit experimental data given a pre-determined model. A model structure is first chosen and

calibrated by adjusting the model parameters until the simulated results fit the experimental ones. The model structure itself is revised if it cannot accurately capture the cell dynamics.

3.2 Procedure of fabricating coin cells and collecting data

3.2.1 Experimental specimen groups

Current rate has significant effect on the rate of aging. [7] To compare the effect of different C-rates on aging, the electrode materials are harvested from unaged batteries and batteries aged with different C-rates. The cells are named by CA-B-D, where A represents the C-rate the battery was aged at, B represents the campaign and D is the SOC setting for that campaign. For modes of campaign, 1 stands for Electric Vehicle (EV), 2 stands for PHEV (Plug-In Hybrid Electric Vehicle), and 3 represents Hybrid Electric Vehicle (HEV). The electrodes of a battery are rolled in application, and different locations are expected to experience different reactions and different degree of aging. To study the variation between different locations, each battery electrode is divided into 5 sections, and four coin cells are fabricated from electrode material from each section. Location 1 is closest to the periphery of the cylindrical battery electrode, and Location 5 is closest to the center of the cylindrical battery. The table below summarizes the different conditions under which each specimen was aged.

Table 1: Matrix of samples for coin cell fabrication based on aging

Cells	C-rate	Campaign	Location

C0	Unaged	Unaged	1,2,3,4,5
C2-1-1	2	EV	1,2,3,4,5
C4-1-1	4	EV	1,2,3,4,5
C7-3-1	~7	HEV	1,2,3,4,5

For the purpose of comparing the anode and cathode from unaged batteries and batteries aged with three different C-rates and variations at five locations along each electrode, a large number of coin cells should be fabricated and tested. Due to the time constraint of my project, only one cell was fabricated and tested. Table 2 summarizes the sample tested in this project.

Table 2: Sample for coin cell testing

Coin Cell	C-rate	Campaign	Electrode	Location
1	~7	HEV	Cathode	3

3.2.2 Coin cell fabrication procedure

As shown in Figure 7, the materials used to assemble the coin cells include a lithium reference electrode, a cathode or anode, a spacer, a spring, and coin cell casings. The spacer is made from stainless steel and used to provide an electrical connection from the electrode to the case. A thin layer of polymer plastic is used as the separator. A ring-shaped spring is placed between the casing and the spacer to exert pressure on the components, press them together and hold them in place.

Figure 7: Components of a coin cell [15]

The materials are first cleaned with isopropyl alcohol. Lithium is highly reactive and reacts with water, so the materials should be free from water vapor as much as possible. We then put samples in the VWR Symphony^{TM} Vacuum Oven for 24 hours to dry, see Figure 8. In order to avoid damaging the materials from high temperature, the oven creates a vacuum environment inside to lower the boiling temperature of water. The temperature is set at 75 Celsius to fully evaporate water adhered to the sample surface.

Figure 8: VWR Symphony™ Vacuum Oven [16]

The materials are then transferred to a LABstar glove box after drying, see Figure 9. The whole assemble process is performed in the glove box in an Argon environment mostly free from oxygen and water. The glove box is constantly monitored by a control panel, and the gage pressure is kept at 2-9 mBar, and the concentration of oxygen and vapor is kept under 5 ppm and 1 ppm respectively. The notation ppm stands for parts-per-million, and is used to describe the concentration of extremely dilute solutions. When the concentrations of water and oxygen are above their limits, the gas inside will be pumped out while Argon will be pumped into the glove box until the concentrations drop below the limits.

Figure 9: LABstar glove box

When materials and tools are being transferred, they are first placed in the chamber at the side of the glove box, as in Figure10. The chamber is open to air at one end and connected to the glove box at the other end, and air tight lids are attached to both ends to seal the chamber when needed. After putting in the materials and tools, the chamber should be sealed at both ends, evacuated, and filled with Argon gas. The procedure should be repeated three times before taking the materials from the chamber to the glove box. This will make sure only an extremely small amount of air goes into the glove box during transferring.

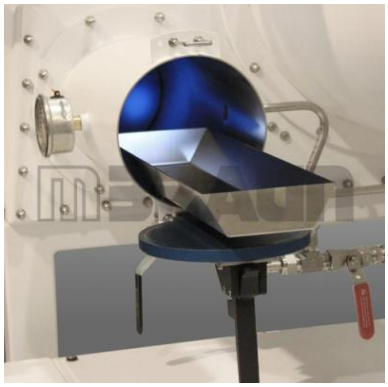

Figure 10: Chamber of LABstar glove box [17]

As shown in Figure 7, when assembling a coin cell, a spring is first placed in the casing. A spacer is placed on top of the spring followed by the cathode. The cathode originally consists of an aluminum current collector that is coated on both sides with the electrode material. One side of the coating must be removed before usage in the coin cell to allow for contact between the current collector and electrolyte. The next step is to place the separator, which should be soaked in electrolyte for 10 to 15 minutes before assembling to ensure enough electrolyte is in the cell in case some electrolyte is leaked before the case can be sealed. Electrolyte is added with a disposable medicine dropper. Due to the high activity

of lithium, water cannot be used as solvent of electrolyte. Instead, the electrolyte is a solution of lithium hexafluorophosphate ($LiPF_6$) in a 1:1 mixture of ethylene carbonate (EC) and dimethyl carbonate (DMC). The anode, the second spacer and casing are positioned in sequence.

After all elements are aligned, the coin cell is sealed with a Compact Hydraulic Crimping Machine (MSK-110), as seen in Figure 11. The pressure is set at 1000psi, and the crimper seals the cell with vertical pressure and pressure along the periphery. After fabrication, the cell is left to settle for at least 12 hours before EIS measurements are taken. This is to allow formation reactions occur and let the system stabilized.

Figure 11: Compact Hydraulic Crimping Machine (MSK-110) [18]

3.2.3 Data collection procedure

The cell is first cycled at a current rate of C/50 during formation cycle to let starting reactions occur. During the testing, the cell is charged and discharged at a current rate of C/20

to keep the system at a steady state. Data were recorded with Gamry Reference 600^{TM} and its built-in software.

To study the battery characteristics during discharging, the cell is discharged from 100% SOC to 0% SOC, and tentatively take EIS measurements at 20% increment of SOC during discharging, namely at 80%, 60%, 40% and 20% SOC. We have an estimate of the cell capacity, and when the cell is cycled at a controlled current rate of C/20, it is estimated to be discharged by 20% in four hours. EIS measurements should be avoided at 100% SOC and 0% because of the unstableness caused by abrupt voltage changes, as shown in Figure 1. Similarly in charging process, we charge the cell from 0% to 100% SOC, and take EIS measurements at 20%, 40%, 60% and 80% SOC.

The measurements process is summarized in Table 3. Note the SOC are estimated according to the theoretically calculated capacity. Terminal voltage, discharging and charging current, and time were recorded each second, and SOC can be determined after the experiment is performed.

Table 3: Testing protocol for discharging and charging

	Discharging current rate: C/20		Charging current rate: C/20	
Step	Test performed	Time	Test performed	Time
1	Discharge from 100% to 80%	4 hr	Charge from 0% to 20%	4 hr
2	EIS measurement		EIS measurement	
3	Discharge from 80% to 60%	4hr	Charge from 20% to 40%	4hr

4	EIS measurement		EIS measurement	
5	Discharge from 60% to 40%	4hr	Charge from 40% to 60%	4hr
6	EIS measurement		EIS measurement	
7	Discharge from 40% to 20%	4hr	Charge from 60% to 80%	4hr
8	EIS measurement		EIS measurement	
9	Discharge from 20% to 0%	4hr	Charge from 80% to 100%	4hr

The four hour time periods may not be completed. To protect the cell, the lower and upper voltage limits are set at 2.5 V and 4.0 V, which correspond to 0% and 100% SOC respectively. When the measured voltage exceeds the limits, the discharging and charging process will stop. When the capacity is below estimation, the voltage will drop below 2.5 V during discharging and rise above 4.0 V during charging before the designed experiment is completed.

When taking EIS measurements, a small sinusoidal excitation signal is imposed on the cell over a frequency range from 1mHz to 100kHz, and the output sinusoidal voltage signal to calculate the impedance response. The small signal generates few changes and keeps the system at steady state. The software calculates and records the real and imaginary impedance at each frequency, and sinusoidal voltage and current are not returned by the software to user. Voltage is measured before and after each EIS measurements to make sure no significant voltage changes occur during EIS test.

The Gamry potentiostat is the hardware used to take measurements. It is a 4-probe instrument, and there are 4 relevant leads that need to be placed in any given experiment.

Working Sense (blue) and Reference (white) measure voltage or potential, and Working (green) and Counter (red) carry the current. [11]

Testing one cell for charging or discharging takes approximately 50 hours. Fortunately, the Sequence Wizard feature in Gamry's Framework allows combining single experiments. The program will automatically advance to the next experiment and execute customized experiments consecutively without the need for manual intervention.

Chapter 4: Results and Discussion

4.1 Experimental results

The charging and discharging profile of open-circuit voltage versus SOC were obtained with measured voltage and calculated SOC. Present capacity is integrated from measured time and current, and SOC is normalized against its maximum capacity. The charging and discharging profile are displayed in Figure 12 and 13 respectively.

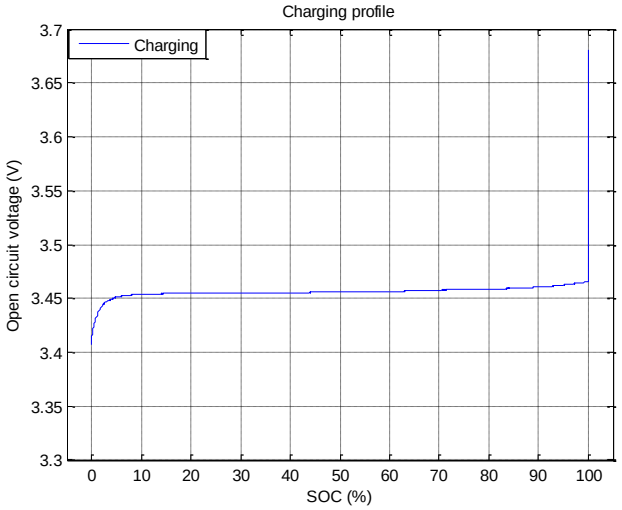

Figure 12: Charging profile for C7 cathode as working electrode

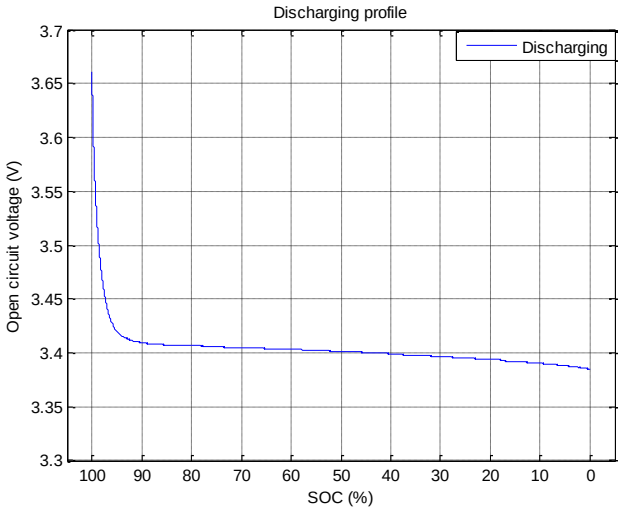

Figure 13: Discharging profile for C7 cathode as working electrode

The EIS curve for C7 with cathode at location 3 as working electrode is obtained at different states of charge for charging and discharging respectively. EIS data were taken at 20%, 40%, 60% and 80% SOC. The actual SOC was calculated after EIS data were taken and was found to match expectations. The complete EIS curves for charging and discharging are displayed in Figure 14.

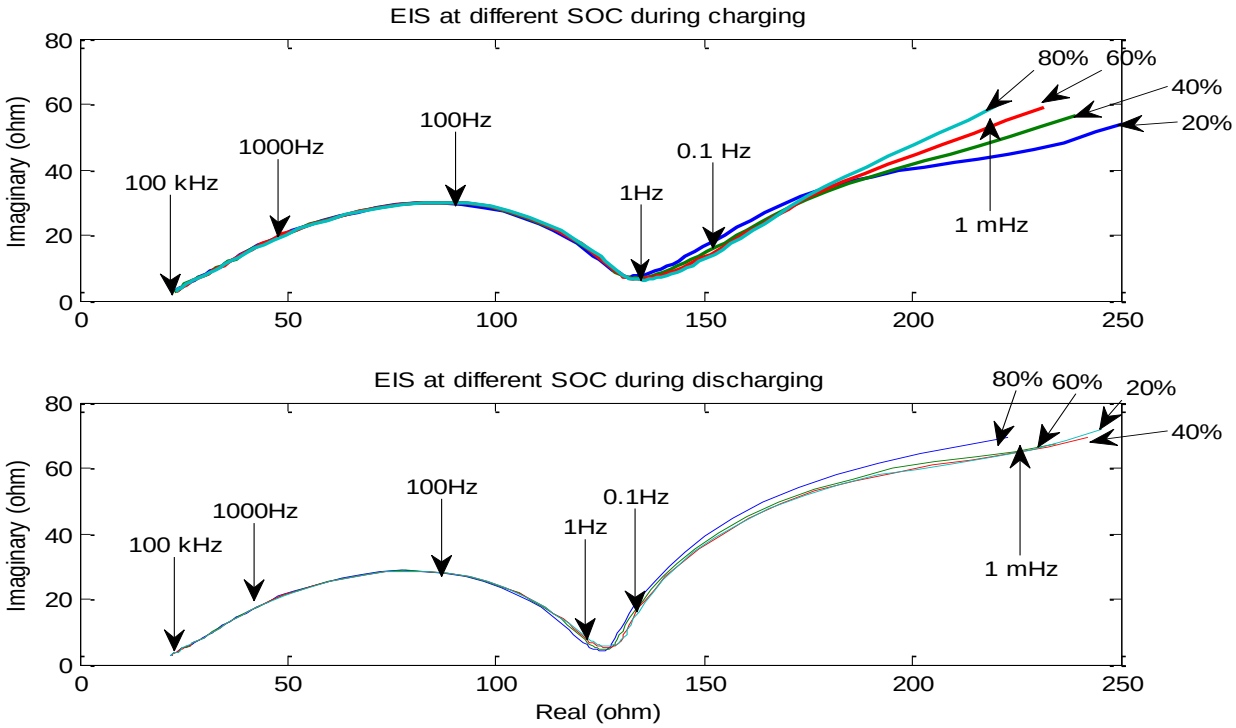

Figure 14: Complete EIS curves for C7 cathode

One curve is mainly composed of a half circle and straight line. The half circle is dominated by behavior at electrode-electrolyte interface, and the straight line is dominated by diffusion. The electrode-electrolyte interface behavior is not expected depend heavily on SOC, while diffusion is expected to be more significant at higher state of charge, and therefore we should have steeper straight line at higher SOC. From the graph, it is observed that diffusion is more significant with increasing SOC for charging process, which matches our expectation. However, the curves for discharging are crowded. It is not obvious whether it is experimental error or general for discharging process, and more experiments are required to draw conclusions with confidence.

The theoretical unaged capacity is calculated from rated capacity of original cylindrical battery according to the manufacturer's manual, and is 4.84 Coulomb for a cathode half cell. During the experiment, neither the charging nor discharging reaches the theoretical capacity, which is expected for the aged cathode. The cell shows a 4.36% capacity fade during charging and a 3.04% capacity fade during discharging. The difference in the capacity between charging and discharging is not understood with the limited amount of testing.

4.2 One-element equivalent circuit model

Simplicity of equivalent circuit model is of critical importance, because calculations need to be performed fast during design and predictions. To start with, a first-order electrical circuit is proposed to model the cell as in Figure 15. V is the voltage source and Load is the external load to complete the circuit. For internal impedance, R_0 represents the electrolyte resistance. The RC element captures the behavior at the electrode surface and electrolyte interface. C_p represents the capacitance of the double layer model due to charge accumulation, and R_p is the lumped resistance of polarization resistance and charge transfer resistance. Transfer function of the internal impedance is represented by equation (10).

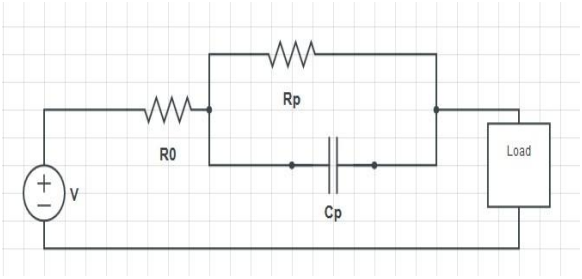

Figure 15: Equivalent circuit model with ideal elements

$$TF = R_0 + \frac{R_P}{sC_pR_p + 1} = \frac{sC_pR_pR_0 + (R_p + R_0)}{sC_pR_p + 1} \qquad (10)$$

The ideal RC element results in a perfect half circle with center on the real axis in Nyquist plot. The R_0 will shift the half circle. However, the experimental EIS curve is an arc with center below real axis, as illustrated in Figure16.

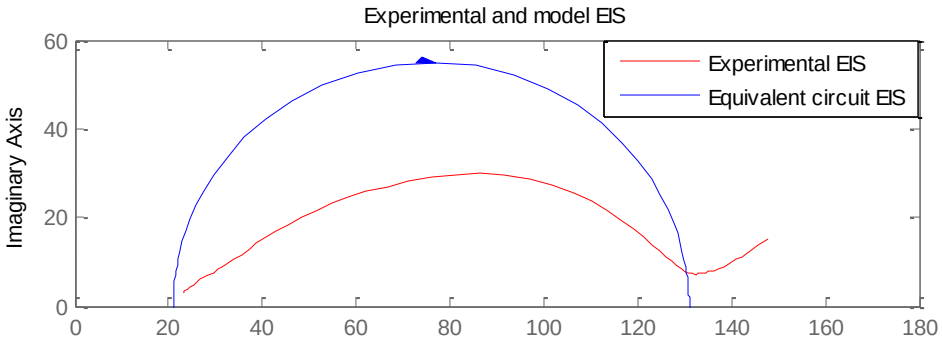

Figure 16: Ideal and real EIS curve

A relaxation process involves conductivity and space charge accumulation and depletion, and an ideal capacitor has a single relaxation time. However in practice, the cell features distributed elements due to surface imperfection, and the relaxation time is not single-valued, but over a range due to surface imperfection, which results in the depressed circular shape of EIS curve. [19] A constant phase element is mathematically equivalent to distributed capacitors, and replaces the capacitor in the circuit. One element refers to one resistor in parallel with a constant phase element.

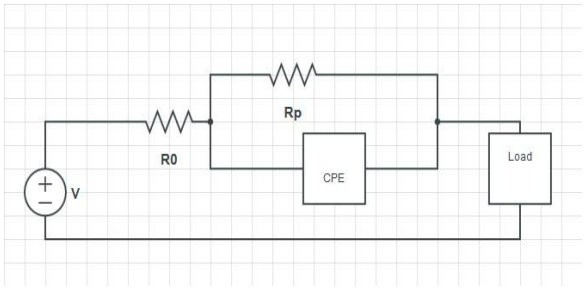

Figure 17: Modified circuit model with constant phase element

The admittance of a constant phase element is commonly expressed in Laplace domain as Y_0*s^a, where Y_0 is a coefficient and a is a fractional exponent between 0 and 1, and the unit of admittance is Siemens. [19] Y_0 and a are both frequency independent. The transfer function of the internal impedance of circuit in Figure 17 is indicated in equation (11).

$$Z(s) = R_0 + \frac{R_p}{s^a R_p Y_0 + 1} \qquad (11)$$

The diffusion tail at the end of the curve is best represented by a Warburg impedance in circuit, and involves a $s^{1/2}$ term in the Laplace domain. A fractional exponent in the transfer function adds to the difficulty and complexity of calculation. The diffusion is dominant at very low frequencies which do not occur often in application. In practice, a frequency above 0.1 Hz is of interest, and we will focus on the modeling and fitting of EIS curves above 0.1Hz with circuit in Figure 17 for now. At most frequencies above 0.1 Hz, the electrode-electrolyte interface is dominant.

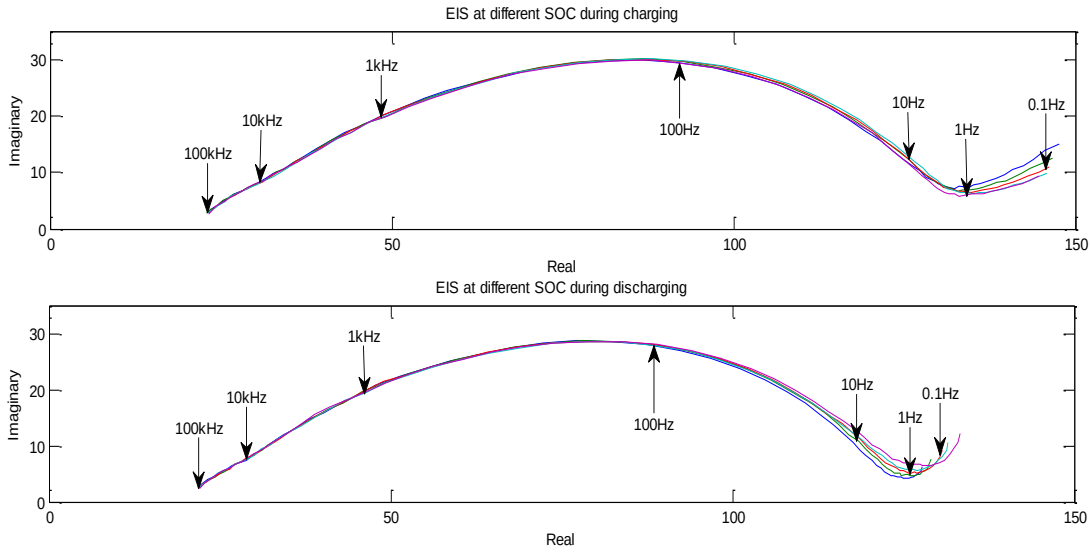

Figure 18: EIS curves for C7 cathode above 1 Hz

4.3 One-element equivalent circuit impedance parameter calibration

4.3.1 Gamry automatic fitting

Echem Analyst is the software built into Gamry to automatically fit the experimental data to frequency-domain plots. Given an electrical model, it will automatically calibrate parameters of the electrical circuit to fit the experimental EIS data. The model editor in *Echem Analyst* enables the user to build and edit electrical circuit, and the "Fit a Model" function will calculate the parameter value of each circuitry element to best fit the experimental EIS data. The selecting tool let the user to perform analysis on selected part of the experimental EIS curve, and the half circle is selected to fit the circuit model. For our model, the parameters to be determined include the series resistance, the parallel resistance

and the constant phase element admittance. The results from Gamry curve fitting is listed in Table 4.

Table 4: Values of parameters for one-element circuit from Gamry curve fitting

	SOC (%)	CPE admittance		Series resistance R_0	Parallel resistance R_p
		Y_0 (S*s^a)*10^6	a*10^3		
Charging	20	201 ±12	541 ±8	21.3 ±0.3	121 ±1
	40	199 ±12	540 ±8	21.4 ±0.3	121 ±1
	60	195 ±12	542 ±8	21.5 ±0.3	121 ±1
	80	193 ±12	541 ±8	21.6 ±0.3	121 ±1
Discharging	20	171 ±11	564 ±8	20.8 ±0.3	108 ±1
	40	166 ±10	569 ±8	21.0 ±0.3	109 ±1
	60	162 ±10	573 ±8	21.1 ±0.3	110 ±1
	80	163 ±10	575 ±8	20.0 ±0.3	111 ±1

An example of Gamry curve fitting result is the experimental and the best fitted EIS curve of C7 cathode at 20% SOC during charging, and is shown in Figure 19. The experimental EIS curve has a diffusion dominated tail from 1Hz to 0.1 Hz, and our model does not include an element to capture diffusion behavior, and the fit deviates from experimental data in this region. Overall, the fit accurately predicts impedance behavior. The goodness of fit is around $700*10^{-6}$ from Non-Linear Least Squares Method (NLLS), shown in equation 12, where σ_i, y_i, and $f(x_i)$ represent the standard deviation of measurement, the data, and the known function respectively. [19]

$$\chi^2 = \sum_{i=1}^{n} [(y_i - f(x_i))/\sigma_i]^2 \quad (12)$$

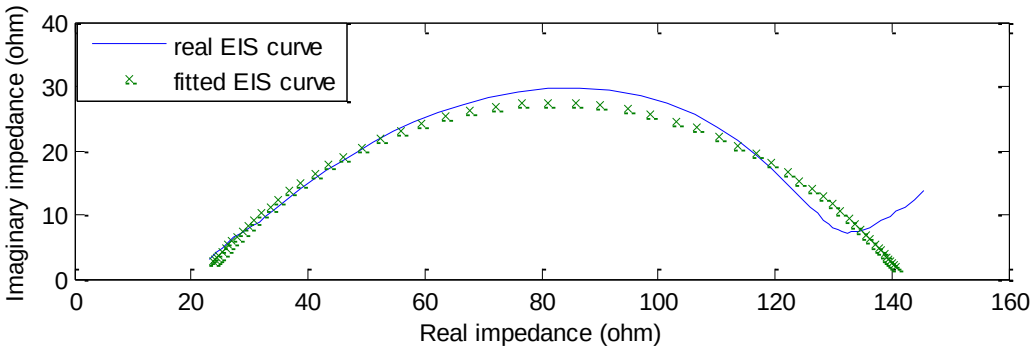

Figure 19: Experimental and Gamry fitted EIS curve of C7 cathode at 20% during charging

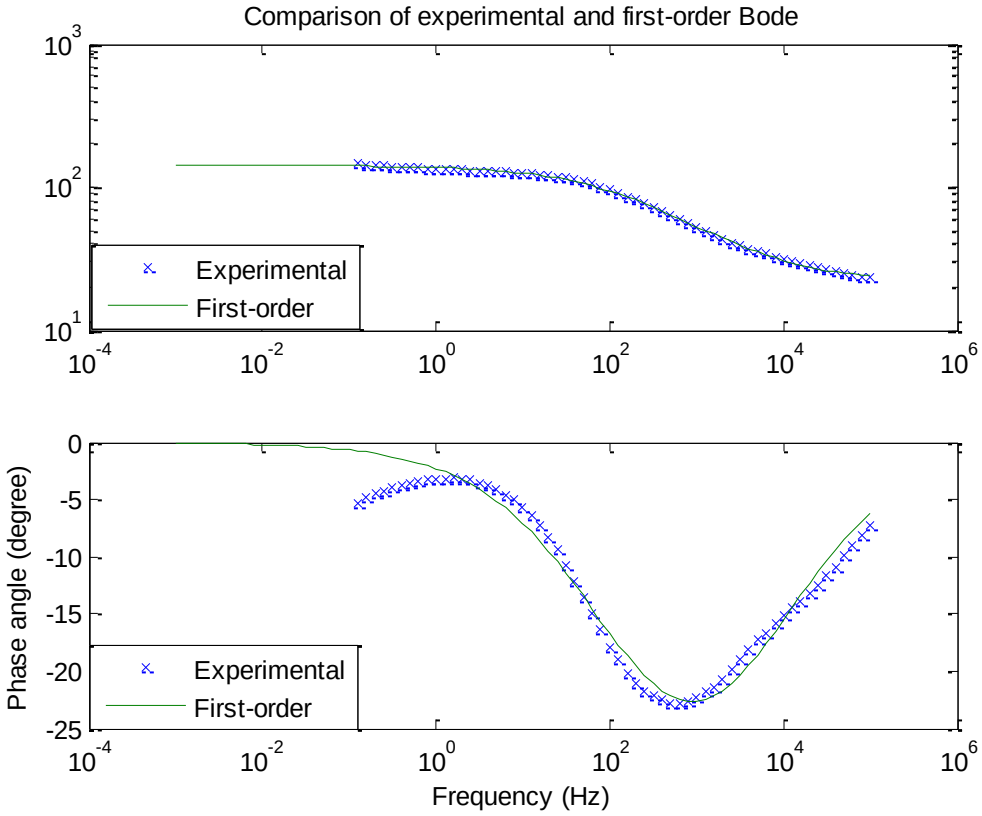

Figure 20: Experimental and Gamry fitted Bode plot of C7 cathode at 20% during charging

From Table 4, the value of each parameter varies slightly with SOC. R_0 is charging and discharging independent as expected because electrolyte has the same resistance for

charge movement in both processes. The parallel resistance is greater for charging than discharging. The voltage at electrochemical equilibrium is denoted by E_r. When there is a current, the electrode potential shifts away from its electrochemical equilibrium potential. During discharging, the potential equals E_r-η_a-η_b, where η_a is the negative shift of anode, and η_b is the positive shift of cathode, and the potential is always less than E_r. During charging, the potential equals E_r+η_a'+η_b', where η_a' is the positive shift of anode, and η_b' is the negative shift of cathode, and the potential is always greater than E_r. [20] During discharging, the reduction of terminal voltage corresponds to an increase in R_p, and in other words, a reduction in terminal voltage.

4.3.2 Pade-approximation

To simplify the expression for internal impedance, the non-linear transfer function of internal impedance could be approximated by a rational function using Pade-approximation. The function to be approximated is equation (11). A general form of Pade function is equation (13). [21]

$$P(x) = \frac{\Sigma_{j=0}^{m} a_j x^j}{1 + \Sigma_k^n b_k x^k} = \frac{a_0 + a_1 x + a_2 x^2 + ... + a_m x^m}{1 + b_1 x + b_2 x^2 + ... + b_n x^n} \qquad (13)$$

We are free to choose the order of the numerator and denominator, and to ensure a proper transfer function, we start by choosing the order of the numerator to be one less than the order of the denominator. There are 4 unknown coefficients in the impedance transfer

function, and to have a clearly defined system, we choose a first-order numerator and second-order denominator, as in equation (14).

$$P(s) = \frac{a_0 + a_1 s}{1 + b_1 s + b_2 s^2} \tag{14}$$

Conventionally to calculate the coefficients in Pade-transfer function, the original impedance function and Pade function are equated at *s*=0, so are first, second, and third derivative. The calculation process is listed as equation (15), (16), (17), and (18).

$$Z(s)|_{s=0} = P(s)|_{s=0} \Rightarrow R_0 + R_p = a_0 \tag{15}$$

$$\frac{d}{ds}(Z(s))|_{s=0} = \frac{d}{ds}(P(s))|_{s=0} \Rightarrow 0 = a_1 - a_0 b_1 \tag{16}$$

$$\frac{d^2}{ds^2}(Z(s))|_{s=0} = \frac{d^2}{ds^2}(P(s))|_{s=0} \Rightarrow 0 = a_0 b_1^{\,2} - a_0 b_2 - a_1 b_1 \tag{17}$$

$$\frac{d^3}{ds^3}(Z(s))|_{s=0} = \frac{d^3}{ds^3}(P(s))|_{s=0} \Rightarrow 0 = a_0 b_1^{\,3} - 2a_0 b_1 b_2 - a_1 b_1^{\,2} + a_1 b_2 \tag{18}$$

Solve for equation (15) through (18), and it is found that a_0 and b_2 are the only determinable coefficients, while a_1 and b_1 can take any value.

$$a_0 = R_s + R_p \tag{19}$$

$$b_2 = 0 \tag{20}$$

This means s=0 is not a good point to evaluate expressions, and another point is needed, and *s*=10 is chosen to be the new evaluation point. After performing calculations, the Nyquist

plots of Pade-approximated and nonlinear function are plotted on the same graph, shown in Figure 21.

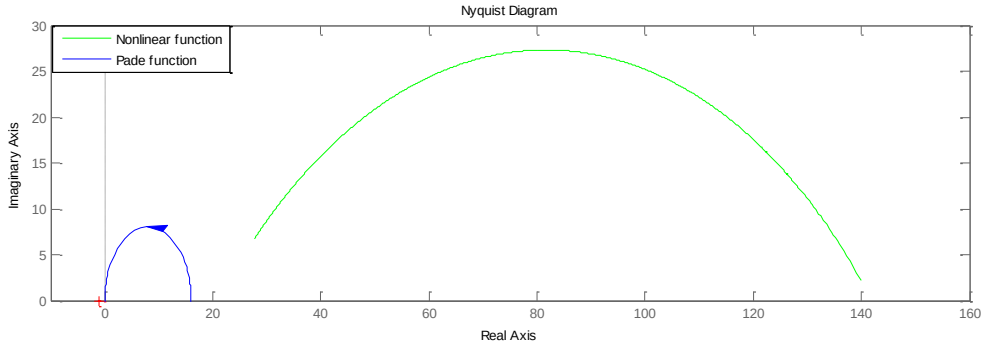

Figure 21: Nyquist plot of nonlinear and Pade-function

The Nyquist plot generated by approximated Pade-function deviates far from the Nyquist plot of nonlinear function. The coefficients that drive the Pade-and nonlinear function equal at one frequency point may generate great errors at other great frequencies. The choice of evaluation point is completely arbitrary, and it is hard to determine the most appropriate point, so the approximation process switches to the least square fitting.

4.3.3 Least square fitting with Pade-function

Another approach is to fit the nonlinear function with Pade-function using least square fitting. At each frequency chosen, the real impedance from nonlinear and Pade-function is determined, and the difference between real impedance of two functions is calculated and squared. At point *k*, the difference is denoted by $D_{\text{real\_k}}$ and the square of difference is denoted by $D_{\text{real\_k}}^2$. The same is done for imaginary impedance, and the square of difference is

denoted by $D_{\text{imag\_k}}{}^2$. If a total of n frequencies are selected, the sum of all square of difference is denoted by Q, and is minimized.

$$\mathrm{Q} = \sum_{i=1}^{n} (Z_{real\_i} - P_{real\_i})^2 + \sum_{i=1}^{n} (Z_{imag\_i} - P_{imag\_i})^2 \qquad (21)$$

To start with, equation (21) is used to approximate the nonlinear function. Figure 24 and 25 show the Nyquist and Bode Pade-function with second order numerator and denominator. The Nyquist plot shows large errors in fitting, but from Bode plot, the Pade-function approximates the nonlinear function.

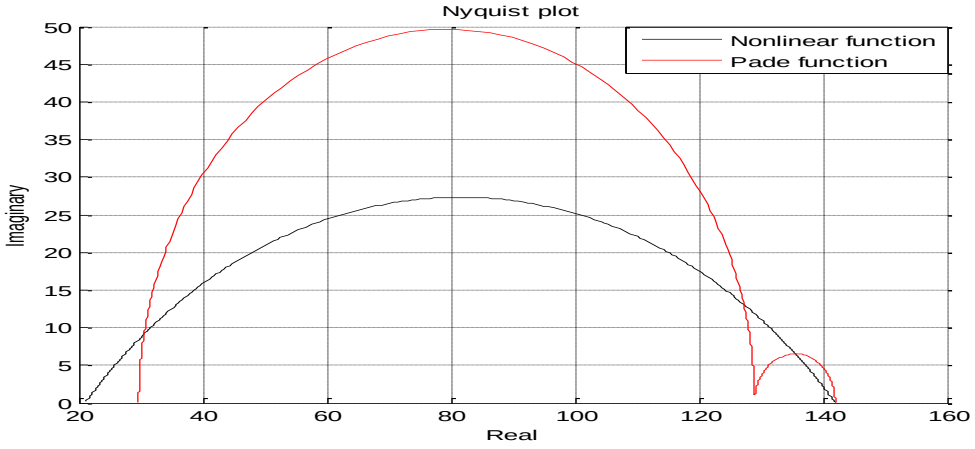

Figure 22: Nyquist plot of Nonlinear and Pade-function from least square fitting

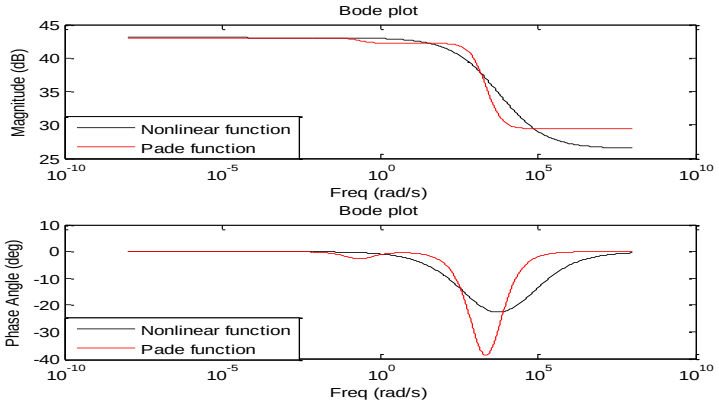

Figure 23: Bode plot of Nonlinear and Pade-function from least square fitting

The reason for the poor fitting is due to the large frequency range, and if the fit is carried out only between 1Hz and 100Hz, the accuracy of fitting is improved as shown in Figures 24 and 25. The step response of the approximation is realistic shown in Figure 26.

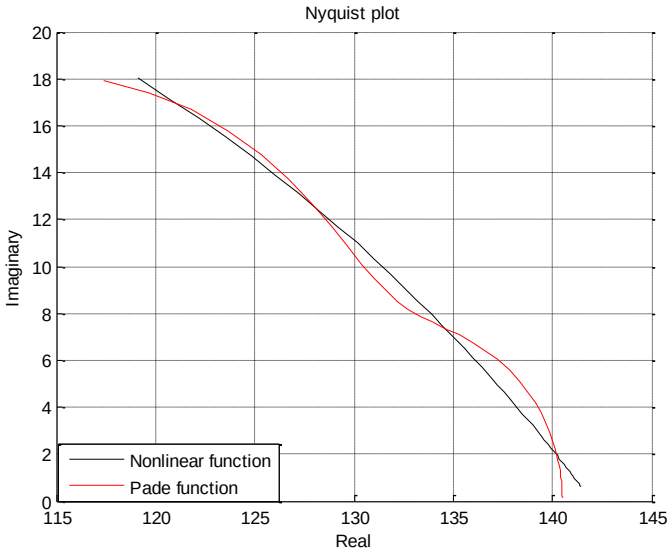

Figure 24: Nyquist plot of nonlinear and Pade-functions

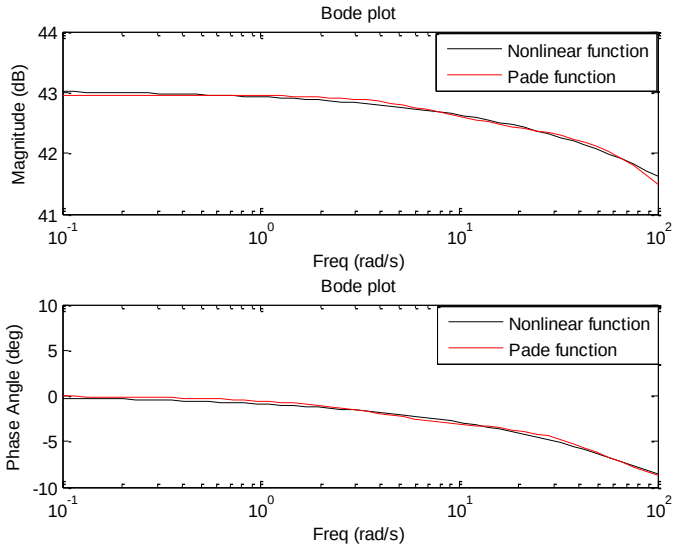

Figure 25: Bode plot of nonlinear and Pade-function

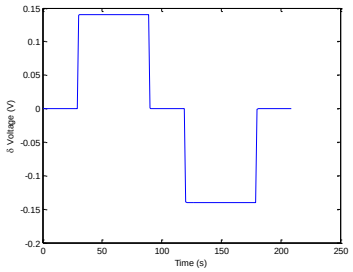

Figure 26: Step response of Pade-function

The same least square fitting can be applied directly to fit the experimental data. The disadvantage of fitting experimental data is the frequency interval cannot be controlled. At frequencies of the most interest, it is desired to have smaller frequency interval to more accurately determine the parameters.

4.4 Two-element equivalent circuit model

A single resistor in parallel with a constant phase element captures the resistive and faradic behavior. As discussed in 2.1, second order captures both concentration and

electrochemical polarization. In general, higher order circuit allows more freedom in fitting. To get more accurate fitting, two elements of a resistor in parallel with a constant phase element are needed in series. The circuit is shown in Figure 27.

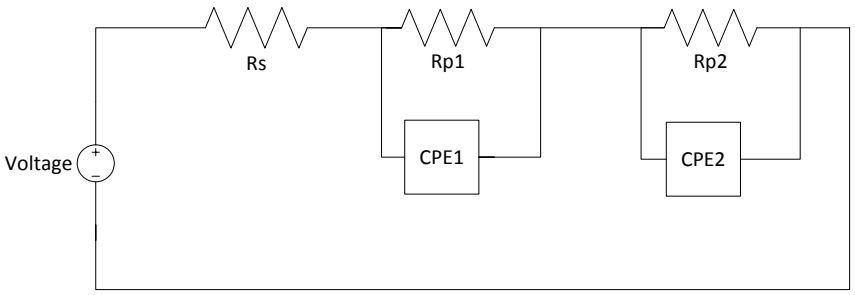

Figure 27: Two-element equivalent circuit model

Similar procedure discussed in section 3.2 is followed to find the parameters of each circuitry element in Echem Analyst. An example of Echem Analyst curve fitting result is shown in Figures 28 and 29, with experimental and the one-element and two-element best fitted EIS curve of C7 cathode at 20% during charging, with two-element circuit parameters summarized in Table 5 summarizes the values, where Y_1*s^($a_{1)}$ (S) is the admittance of CPE_1 and the Y_2*s^(a_2) (S) is the admittance of CPE.

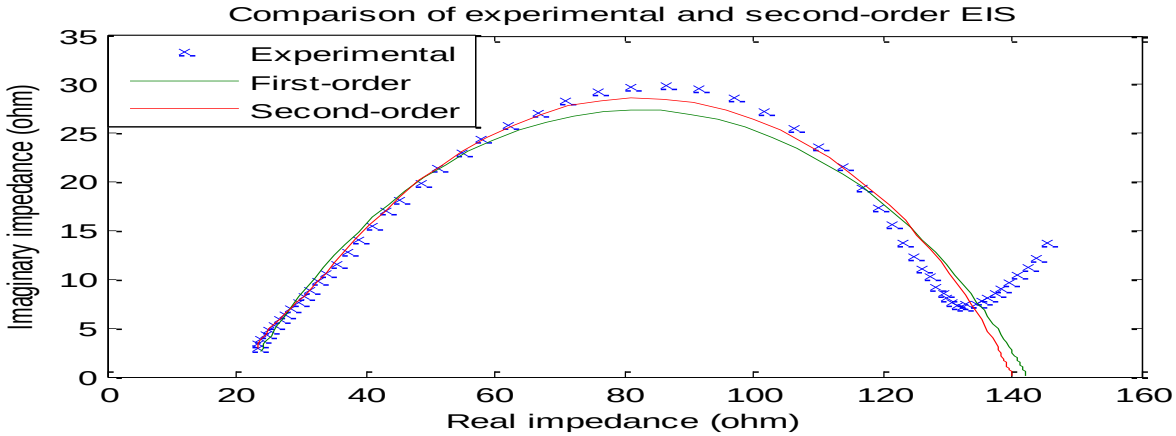

Figure 28: Experimental and Gamry fitted EIS curve of C7 cathode at 20% during charging

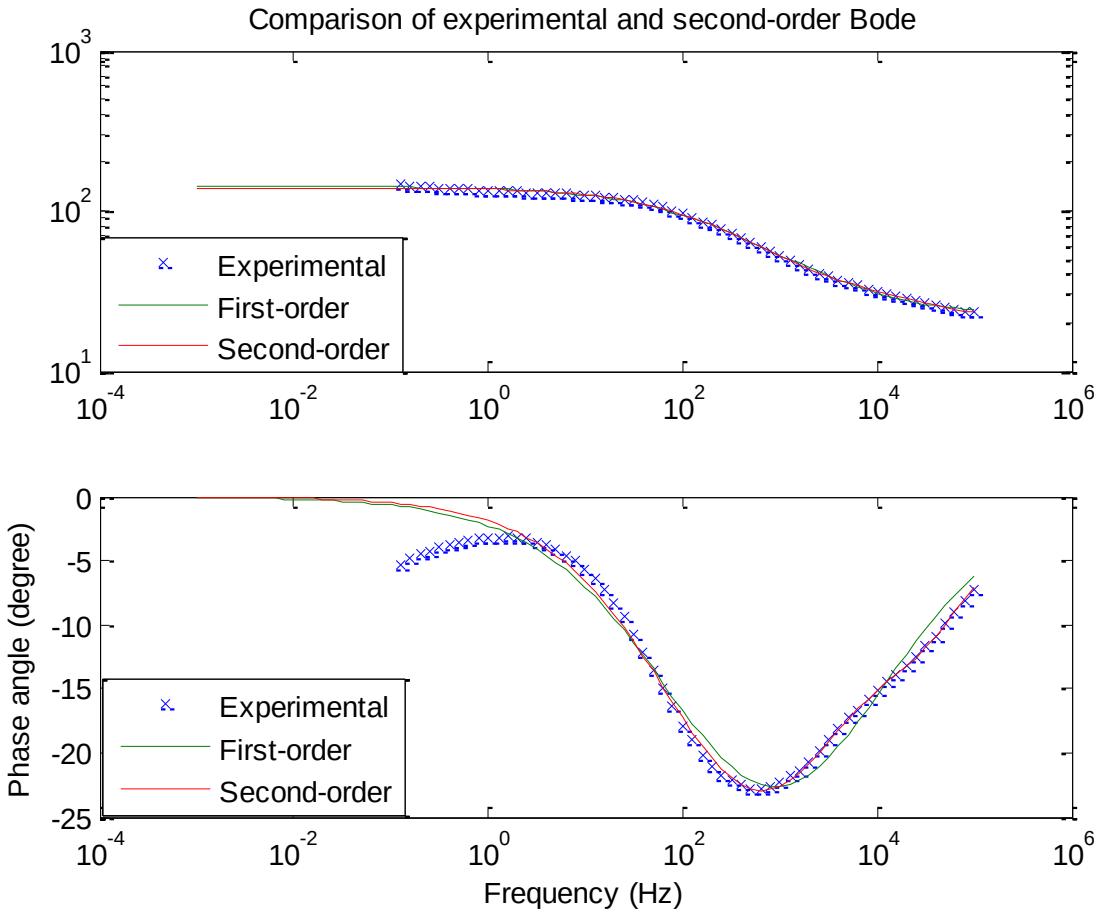

Figure 29: Experimental and Gamry fitted Bode curve of C7 cathode at 20% during charging

Table 5: Parameters for two-element circuit from Gamry curve fitting

C7 Cathode during charging at 20% SOC		
R_s (ohm)		21.3 ±0.7
R_{p1} (ohm)		115 ±3
Y_1*s^(a_1) (S)	Y_1 (S)*10^6	156 ±17
	a_1*10^3	587 ±20
R_{p2} (ohm)		3.8 ±2.3
Y_2*s^(a_2) (S)	Y_2(S)*10^6	311 ±10

	a_2*10^3	948 ± 311

From the Bode plot, one-element and two-element magnitudes all match well with the experimental magnitudes, and two-element angle shows slight improvement over one-element in fitting experimental phase angle. The goodness of fit for a first order equivalent circuit is around $700*10^{-6}$, while that for a two-element equivalent circuit is around $500*10^{-6}$. A two-element circuit improves the accuracy in predicting impedance behavior, but introduces a second fractional exponent.

4.5 Voltage calibration

During charging and discharging, the voltage changes extremely slowly over a large range of SOC, from 5% to 95%. The voltage change of this range is only approximately 0.2% of the maximum voltage, and the voltage can be approximated by a constant 3.457V during charging and 3.401V during discharging for this region. Terminal voltage should be larger during charging than discharging as discussed in 4.3.1.

When the cell is charged and discharged at infinitesimal current, the terminal voltage is the open-circuit voltage, which is the value of the voltage source in the model. The cell is charged at C/20, and the difference between charging and discharging voltage is around 2% of the voltage in flat range. For the purpose of finding the open-circuit voltage, the difference is small and an average is taken. Therefore, the open-circuit of model in Figure 17 is 3.43V.

Chapter 5: Conclusion and Recommendation for Future Work

5.1 Conclusion

An equivalent circuit was developed to model the behavior of a Li-ion half cell at the interested frequency range for vehicle application. The calibration of the equivalent circuit model was based on the charging and discharging profile and EIS measurements. The circuit comprises of an ideal voltage source, an external load, a resistance in parallel with a constant phase element, together in series with a resistor. A second element of resistance in parallel with constant phase element improves the accuracy of fitting, but introduces more complexity, and is not recommended. In this project the parameters are obtained through Gamry automatic fitting tool. The cell has smaller internal impedance during discharging than charging. The governing equation of the non-linear system can be approximated by a Pade function with second-order numerator and denominator, which allows fast calculations during design. The disadvantage of Pade function is that coefficients in the function do not have a physical meaning.

One major drawback of the project is that the internal impedance and terminal voltage behavior of a cell is heavily dependent on the system frequency. However, the system frequency is hard to estimate. For example, when the car stops, the thermal energy from braking is converted to electric power through generator, but the charging frequency is uncertain.

5.2 Recommendation for future work

Given the small number of samples, the model could not be validated with more data sets. Future work should be done to fabricate and test additional coin cells. A close alignment between results from developed model and new experimental results indicates a good model. In the future, EIS data should also be taken at 5% and 95% SOC to capture system behavior at very low and high SOC.

Coin cell should be fabricated from electrode materials aged under other conditions, and the effects of aging current, location on electrode, and different aging campaign should be compared. In a hybrid vehicle, the battery voltage and current are constrained. With more cell testing, the maximum allowable current for long-time and a short period can be identified, and implemented in control design.

It is desired to develop a model for the battery system frequency under different driving conditions, and with respect to the condition of generator and regeneration system. With an estimate of the charging and discharging frequency, the battery performance can be better predicted.

References:

[1] Simon Robinson, “The Dozen Most Important Cars of All Time-Toyota Prius (1997-present),”*Time* (2007)

[2] Richard S. Chang, “Sportier but Thirstier, a Hybrid Honda Tries to Be Hip,”*The New York Times* (2010)

[3] Bryan Walsh, “The History of the Electric Car-Green Motors,”*Time* (2007)

[4] C. Liao, H. Li, L. Wang, “A Dynamic Equivalent Circuit Model of LiFePO4

Cathode Material for Lithium Ion Batteries on Hybrid Electric Vehicles”, *Vehicle Power and Propulsion Conference* (2009)

[5] MIT Electric Vehicle Team, “A Guide to Understanding Battery Specifications” (2008).

[6] J. Belt, V. Utgikar, I. Bloom, “Calendar and PHEV cycle life aging of high-energy, lithiumion cells containing blendedspinel and layered-oxide cathodes,”*Journal of Power Sources* **196,**10213– 10221(2011).

[7] G. Ning, B. Haran, B.N. Popov, “Capacity fade study of lithium-ion batteries cycled at high discharge rates”, *Journal of Power Sources* **117,** 160-169 (2003)

[8] E. Barsoukov, J. Macdonald, “Impedance Spectroscopy Theory, Experiment, and Applications” 2005

[9] L. Faulkner, “Understanding Electrochemistry: Some Distinctive Concepts”, University of Illinois

[10] Andrzej Lasia, “Electrochemical Impedance Spectroscopy and its Applications”, *Modern Aspects of Electrochemistry,* Volume 32, pp143-248 (2002)

[11] Gamry Instrument, “Technical Note Two-, Three-, and Four Electrode Experiments”

[12] Liaw, B. Y., Nagasubramanian, G., Jungst, R. G., Doughty, D. H., “Modeling of Lithium Ion Cells - A simpleequivalent-circuitmodel approach,” *Solid State Ionics* **175,** 835-839 (2004).

[13] H. He, R. Xiong, J. Fan, “Evaluation of Lithium-Ion Battery Equivalent Circuit Models for State of Charge Estimation by an Experimental Approach”, *Energies,* 4, 582-598 (2011)

[14] D. Evans, K. O’Connell, R. Petersen, M. Kelly, “Cyclic Voltammetry”, University of Wisconsin-Madision

[15] MTI Corporation, http://mtixtl.com/

[16] VWR, “VWR® symphony™ Vacuum Ovens”, https://us.vwr.com/

[17] MBraun, http://www.mbraunusa.com/

[18] MTI Corporation, “Compact Hydraulic Crimping Machine”, http://mtixtl.com/

[19] V. Birss, D. Truax, “ An Effective Approach to Teaching Electrochemistry”, The University of Calgary

[20] J. Forman, S. Bashash, J.Stein, H. Fathy, “Reduction of an Electrochemistry-Based Li-Ion Battery Model via Quasi-Linearization and Pade ´Approximation”, *Journal of The Electrochemical Society*, **158**, 2011